

1 **Detection of delay in post-monsoon agricultural burning across** 2 **Punjab, India: potential drivers and consequences for air quality**

3 Tianjia Liu^{1*}, Loretta J. Mickley^{2*}, Ritesh Gautam³, Manoj K. Singh⁴, Ruth S. DeFries⁵,
4 and Miriam E. Marlier⁶

5 ¹Department of Earth and Planetary Sciences, Harvard University, Cambridge, MA, 02138, USA

6 ²School of Engineering and Applied Sciences, Harvard University, Cambridge, MA, 02138,
7 USA

8 ³Environmental Defense Fund, Washington, D.C., 20009, USA

9 ⁴University of Petroleum and Energy Studies, Dehradun, Uttarakhand, India

10 ⁵Department of Ecology, Evolution, and Environmental Biology, Columbia University, New
11 York, NY, 10027, USA

12 ⁶RAND Corporation, Santa Monica, CA, 90401, USA

13

14 *Correspondence to: Tianjia Liu (tianjialiu@g.harvard.edu), Loretta Mickley
15 (mickley@fas.harvard.edu)

16 **Abstract**

17 Since the Green Revolution in the mid-1960s, a widespread transition to a rice-wheat
18 rotation in the Indian state of Punjab has led to steady increases in crop yield and productivity.
19 After harvest of the monsoon rice crop, the burning of excess crop residue in Punjab from
20 October to November allows for rapid preparation of fields for sowing of the winter wheat crop.
21 Here we use daily satellite remote sensing data to show that the timing of peak post-monsoon fire
22 activity in Punjab and regional aerosol optical depth (AOD) has shifted later by approximately
23 two weeks in Punjab from 2003-2016. This shift is consistent with delays of 11-15 days in the
24 timing of maximum greenness of the monsoon crop and smaller delays of 4-6 days in the timing
25 of minimum greenness during the monsoon-to-winter crop transition period. The resulting
26 compression of the harvest-to-sowing period coincides with a 40% increase in total burning and
27 50% increase in regional AOD. Potential drivers of these trends include agricultural
28 intensification, variations in monsoon rainfall, and a recent groundwater policy that delays
29 sowing of the monsoon crop. The delay and amplification of burning into the late post-monsoon
30 season suggest greater air quality degradation and public health consequences across northern
31 India.

32 **1. Introduction**

33 Rapid increases in mechanized harvesting in the Indo-Gangetic Plain (IGP) since the
34 mid-1980s, together with steady increases in crop production, have led many farmers to burn the
35 abundant residue left behind by this practice (Badarinath *et al* 2006). Such burning is a quick,
36 cheap, and efficient method to ready the fields for the next crop. However, the smoke from post-
37 monsoon crop residue burning, primarily during October to November, amplifies severe haze
38 events in the region (Kaskaoutis *et al* 2014), such as that observed in early November 2016
39 (Cusworth *et al* 2018). Of particular concern is the observed increase in aerosol loading
40 associated with an upward trend in post-monsoon burned area and with a shift toward a later

41 peak in post-monsoon fires in northwestern India (Thumaty *et al* 2015, Jethva *et al* 2018, Liu *et*
42 *al* 2019). Here we use daily satellite remote sensing data to better quantify the temporal shift
43 toward later burning in the state of Punjab, the “breadbasket” of India. Such a shift would have
44 implications for air quality, since peak burning is more likely to coincide with meteorological
45 conditions that are favorable in amplifying persistent haze.

46 Agricultural intensification of rice and wheat in India has led to over two-fold and three-
47 fold increases, respectively, in crop yield since the Green Revolution in the mid-1960s. In the
48 western IGP, the predominant rice-wheat rotation is highly productive (Kumar *et al* 2015).
49 Punjab, an agricultural state in northwestern India, contributes more than one-fifth of rice and
50 one-third of wheat to the central grain pool in India, and thus generates large amounts of crop
51 residue annually. Since the mid-to-late 1980s, farmers have increasingly used mechanized
52 harvesting methods in preference to sickle-based manual harvesting in order to reduce labor
53 costs and save time (Badarinath *et al* 2006, Kumar *et al* 2015). The use of combine harvesters,
54 however, leaves behind an abundance of scattered and root-bound residue that is difficult to
55 remove and thus often burned post-harvest to prepare for timely sowing of the next crop (Kumar
56 *et al* 2015). The burning allows for quick disposal of crop residues and shortens the harvest-to-
57 sowing transition from the *kharif* (monsoon crop) to *rabi* (winter crop) season. A quicker
58 transition between crops also allows for earlier sowing of wheat during post-monsoon to avoid
59 springtime heat (Lobell *et al* 2013).

60 However, the burning of post-monsoon rice residue can severely degrade air quality
61 downwind of the agricultural fires over the IGP (Badarinath *et al* 2006, Kaskaoutis *et al* 2014,
62 Liu *et al* 2018b, Cusworth *et al* 2018, Jethva *et al* 2018). In particular, smoke from rice residue
63 burning in October and November may account for more than half the fine particulate matter
64 (PM_{2.5}) concentrations in the Delhi National Capital Region (Cusworth *et al* 2018), which
65 already experiences intense urban pollution from local and other regional sources (Amann *et al*
66 2017). A temporal shift in fire activity to later in the year could exacerbate air quality
67 degradation since late autumn-to-winter meteorology in the IGP favors smog formation due to
68 weak winds, frequent temperature inversion, and a shallow boundary layer (Choudhury *et al*
69 2007, Saraf *et al* 2010, Liu *et al* 2018b).

70 Observations from the Moderate Resolution Imaging Spectroradiometer (MODIS),
71 aboard NASA’s Terra and Aqua satellites, have been extensively used to investigate fire activity,
72 crop yields, production, and phenology, and land use change detection. However, MODIS multi-
73 day composites (8-day, 16-day) typically analyzed are insufficient to capture and resolve rapid
74 changes in crop phenology (Zhao *et al* 2009). Here we use daily active fire and surface
75 reflectance data from MODIS to investigate trends in agricultural activity in Punjab. Specifically,
76 we quantify the delays in post-monsoon agricultural fire activity and determine whether the
77 seasonal cycle of monsoon to post-monsoon vegetation greenness reveals similar delays. We
78 conclude with a discussion of the potential drivers of these interannual changes and an analysis
79 of the consequences for regional air quality.

80 **2. Data and Methods**

81 *2.1 Study region*

82 The IGP is home to over 700 million people (appendix S1.4), many of whom rely on
83 agricultural productivity of the densely cropped belt of northern India and parts of Pakistan,

84 Nepal, and Bangladesh for livelihood and food security. Relative to other double-cropped states
85 in northern India, such as Haryana, Uttar Pradesh, and Bihar, Punjab has the highest rice-wheat
86 productivity (Kumar *et al* 2015) and is spatially more homogenous in terms of fire intensity
87 (Figure 1a), rice-wheat yields, and topography (Azzari *et al* 2017). Here we focus on Punjab
88 during the post-monsoon rice residue burning season (defined here as September 20 to
89 November 30), when fields are prepared for winter wheat sowing. To a lesser degree, we
90 examine the pre-monsoon wheat residue burning season (April 1 to May 31), when fields are
91 prepared for monsoon rice sowing (Figure 1b).

92 2.2 Active fires and vegetation indices

93 For analysis of fire activity, we sum daily 1-km maximum Fire Radiative Power (FRP), a
94 proxy for fire intensity, derived from MODIS/Terra and Aqua (MOD14A1/MYD14A1,
95 Collection 6). We also compare FRP with MODIS-derived fire counts and burned area and
96 MODIS-based fire emissions from the Global Fire Emissions Database, version 4 with small
97 fires (GFEDv4s) (Table S1). For analysis of vegetation greenness, we use daily 500-m
98 MODIS/Terra surface reflectance (MOD09GA, Collection 6) to derive two vegetation indices,
99 the Normalized Difference Vegetation Index (NDVI) and Normalized Burn Ratio (NBR):

$$100 \quad \text{NDVI} = \frac{\rho_2 - \rho_1}{\rho_2 + \rho_1} \quad (1)$$

$$101 \quad \text{NBR} = \frac{\rho_2 - \rho_7}{\rho_2 + \rho_7} \quad (2)$$

102 where ρ_i is the surface reflectance of MODIS band i . The wavelength range of the bands is as
103 follows: 620-670 nm for band 1 (red), 841-876 nm for band 2 (near infrared), and 2105-2155 nm
104 for band 7 (shortwave infrared). These active fire and surface reflectance datasets are described
105 in more detail in appendix S1.

106 2.3 Statistical analysis

107 We estimate linear trends with residuals bootstrapping. Unlike the linear regression t-test,
108 which assumes that the residuals are normally distributed, bootstrapping preserves and resamples
109 from the sample residuals distribution. To obtain a sample distribution, 1000 iterations are
110 performed in which residuals are randomly sampled with replacement for each iteration and the
111 dependent variable y re-fit using linear regression.

112 2.3.1 Characterizing the temporal progression of agricultural fires

113 We characterize the progression of the pre-monsoon and post-monsoon burning seasons,
114 defined in Section S2.1, of each year in order to assess interannual temporal trends. While the
115 moderate spatial resolution of MODIS likely leads to large underestimates in total post-monsoon
116 agricultural fire activity in northwestern India (Liu *et al* 2019), here we aim to quantify linear
117 trends using the relative temporal distribution of fire intensity, which is minimally impacted by
118 spatial resolution (appendix S1.1). To estimate the midpoint date of each burning season,
119 $x(\text{FRP})_{\text{midpoint}}$, we weight each day of the burning season, from 1 to n total days, by the
120 corresponding daily sum of Terra and Aqua MODIS FRP and take the average. We approximate

121 the timing of the start and end date of burning for that season, $x(FRP)_{start}$ and $x(FRP)_{end}$, as
122 $x(FRP)_{midpoint} \pm 1.5\sigma$, where σ , also weighted by daily FRP, is one standard deviation.

123 The value $x_{midpoint}$ may not correspond to the day of peak burning, $x(FRP)_{peak}$. To
124 estimate x_{peak} , we fit Gaussian density curves to daily FRP, thus smoothing potential noise in
125 FRP due to inconsistencies in observing area caused by cloud and haze cover:

$$126 \quad g(x) = k \cdot e^{-0.5[(x-\mu)/\sigma]^2} \quad (3)$$

127 where $g(x)$ is the Gaussian function, x is days of the burning season expressed as 1 to n total
128 days, m is the mean of x , σ is the standard deviation of x , and k is an arbitrary scaling parameter.
129 We then use the *optim* function from the R *stats* package to minimize non-linear least squares of
130 $g(x)$ and y , or fractional daily FRP, and to estimate the μ , σ , and k parameters that yield the
131 optimal Gaussian fit. As first guesses of the three parameters for the *optim* function, we use
132 $x(FRP)_{midpoint}$ as μ , 7 as σ , and 1 as k .

133 2.3.2 Tracking crop phenology with NDVI and NBR

134 NDVI is widely used to characterize the cycling in vegetation growth, land cover change,
135 and crop productivity (Yengoh *et al* 2015, Justice *et al* 1985). NBR, while typically used in
136 burned area and burn severity classification (Key and Benson 2006), is analogous to NDVI,
137 which relies on the visible red reflectance instead of the shortwave infrared (SWIR) reflectance.
138 A major advantage of NBR is that compared to visible wavelengths, SWIR wavelengths can
139 better discriminate between vegetation and bare soil (Chen *et al* 2005, Asner and Lobell 2000)
140 and are less susceptible to atmospheric interference from smoke aerosols and thin clouds (Roy *et al*
141 *al* 1999, Eva and Lambin 1998, Avery and Berlin 1992). Here we use NBR as a complement to
142 NDVI to track crop phenology with variations in vegetation greenness.

143 We estimate the timing of crop maturation, or maximum greenness, during the monsoon
144 growing season with both the daily median NDVI and NBR time series. Assuming that the
145 seasonal progression in the crop cycle is similar across years, the timing of peak greenness in the
146 growing season diagnoses the timing of the overall growing season. To estimate the timing of the
147 maximum monsoon greenness with the noisy daily time series, we apply weighted cubic splines
148 smoothing with bootstrapping on time steps within a defined window that straddles the day of
149 monsoon peak greenness. Cubic splines smoothing stitches together piecewise third-order
150 polynomial interpolation between “knots,” or selected experimental points, and has been used
151 extensively for crop phenology applications (Jain *et al* 2013, Mondal *et al* 2014, 2015, Jain *et al*
152 2017). We apply weights to the NDVI and NBR time series using the daily fraction of “usable”
153 pixels, or those uncontaminated by clouds or thick haze (hereafter referred to as usable fraction)
154 in the study area. This weighting follows from our greater confidence in daily median NDVI and
155 NBR on clearer days versus cloudier and/or hazier days. Prior to bootstrapping, we make initial
156 guesses of the four local maxima and minima: monsoon and winter peak greenness and pre-
157 monsoon and post-monsoon trough greenness. We use these initial guesses to center a window of
158 300 days. Using a smoothing parameter of 0.75, we smooth the vegetation index time series with
159 weighted cubic splines within the defined window and estimate the bootstrapped mean timing of
160 maximum NDVI or NBR for each year. We repeat this process to estimate the earliest date when
161 fields are ready to sow the winter crop, or trough greenness, during the post-monsoon transition

162 period.

163 To further assess whether the 2008-09 policy implementations led to abrupt shifts in
164 monsoon peak greenness or post-monsoon trough greenness, we quantify the mean difference
165 between the 2003-2007 and 2008-2016 time periods. As we will see, the observed shifts are
166 primarily localized in 2 years from 2008-09 with little change thereafter, and so the overall linear
167 trend may overestimate delays in peak or trough greenness. To find the mean delay, we use
168 weighted two-sample t-tests with bootstrapped statistics. The weights are $1/\sigma^2$, in which σ is
169 associated with bootstrapped estimates of the timing in peak or trough greenness over the two
170 time periods.

171 2.3.3 Regional aerosol optical depth exceedances

172 To quantify enhancements in regional air quality degradation during the post-monsoon
173 burning season, we use MODIS/Terra Deep Blue retrievals of aerosol optical depth (AOD) over
174 Punjab, Haryana, Delhi, and western Uttar Pradesh (i.e., encompassing the aerosol source and
175 downwind transport regions of the IGP; [appendix S1.3](#)). In order to minimize the contribution of
176 background AOD, we analyze regionally averaged AOD “exceedances” – that is, the daily
177 spatial mean of AOD increments above the mean $\text{AOD} \pm 1\sigma$ for each pixel and season across
178 Punjab, Haryana, Delhi, and western Uttar Pradesh. We analyze these daily mean AOD
179 exceedances within the $x(\text{FRP})_{start}$ and $x(\text{FRP})_{end}$ window to isolate the effect of agricultural
180 burning. To estimate the timing of peak AOD exceedances, or $x(\text{AOD})_{peak}$, we apply Gaussian
181 density curve optimization to values within this window expanded by two weeks. Such
182 expansion ensures that the optimization is not thrown off by high AOD days isolated at the
183 beginning or end of the season.

184 3. Results

185 3.1 Trends in seasonal agricultural fire activity

186 The bimodal distribution of peak agricultural fire activity in both pre-monsoon and post-
187 monsoon periods is limited to northwestern India, primarily in Punjab, as well as northern
188 Haryana ([Figures 1, S1](#)). Generally, 90% of post-monsoon fires in Punjab are set within an
189 approximate four-week window (27 ± 3 days) from mid-October to early November. We
190 estimate that the timing of peak post-monsoon fire intensity has shifted later in Punjab by 1.17
191 days yr^{-1} , statistically significant at the 95% confidence interval (CI), indicating that the burning
192 of rice residue has shifted later by over two weeks from 2003-2016 ([Figure 2, Table S2](#)). These
193 findings are corroborated by similar temporal and magnitude shifts in GFEDv4s fire emissions
194 and MODIS fire counts and burned area ([Table S3](#)). In contrast, we find no such statistically
195 significant delays in the pre-monsoon burning season in Punjab ([Table S2](#)).

196 Spatially, the post-monsoon temporal shift is larger in magnitude in districts in western
197 Punjab than in eastern Punjab ([Figure S3](#)). Moreover, the 14-year trends in total fire intensity for
198 each 3-day block within this window signal a shift in the peak burning period, with decreasing
199 FRP in mid-to-late October and increasing FRP in early November ([Figure 2](#)). We estimate that
200 the magnitude of the peak fire activity, indicated by the 99th percentile of 3-day block sums of
201 FRP, has doubled over the 14-year period, an increase that may be partly attributed to some
202 homogenization in the timing of burning across districts.

203 3.2 Trends in vegetation greenness from monsoon to post-monsoon

204 We also examine whether vegetation greenness in Punjab show similar shifts during the
205 monsoon growing season and post-monsoon harvest-to-sowing transition period. Whereas the
206 timing of minimum NBR and NDVI occurs after near-completion of post-monsoon burning in
207 mid-to-late November, the temporal maximum of these vegetation indices occurs near the end of
208 the monsoon around late August or early September (Figure 1b), indicating crop maturation. In
209 Punjab, the timing of maximum NDVI and NBR shows an overall delay of 11-15 days, with a
210 large, abrupt shift of 7-9 days from 2008, relative to previous years (Figure 3a-b). Concurrently,
211 there is an evident increasing trend in maximum monsoon NBR (0.06 decade^{-1} , 95% CI: [0.04,
212 0.08]) and NDVI (0.07 decade^{-1} , 95% CI: [0.05, 0.09]), consistent with steady increases in
213 annual total *kharif* rice production in Punjab of 0.13 Tg yr^{-1} (95% CI: [0.09, 0.17]) (Figures 3b,
214 S4, Table S5). Such increases in peak NBR and NDVI also suggest greater quantities of crop
215 residue, which may lead to amplified fire intensity and emissions. In contrast to the shift in
216 maximum NBR and NDVI, we find a smaller delay of 4-6 days in the timing of the minimum
217 values of these indices during post-monsoon (Figure 3c-d, Table S5), indicating that the shift in
218 the monsoon growing season is greater than the corresponding shift in the timing of the earliest
219 date when fields are ready for winter wheat sowing. In addition, we find that the duration from
220 the start of the burning season to trough post-monsoon greenness has decreased by $0.77 \text{ days yr}^{-1}$
221 (95% CI: [-1.14, -0.41]), providing evidence for a shortened harvest-to-sowing period (Figure
222 S5). Taken together, our results suggest that the temporal shifts in post-monsoon burning are
223 likely associated with later sowing and harvesting of the monsoon crop.

224 3.2.1 The utility of NBR as a vegetation index

225 We have so far considered NBR and NDVI as complementary vegetation indices. Here
226 we further demonstrate the utility of NBR for tracking crop phenology, particularly in resolving
227 the troughs of the crop cycle. The weaker detrended correlations ($r = 0.23 \pm 0.39$) between the
228 two vegetation indices during transition months between the *kharif* and *rabi* seasons (May, June,
229 October, and November) compared to other months ($r = 0.88 \pm 0.12$) support the notion that
230 NDVI more poorly resolves and tends to “flatten” the troughs of the double-crop cycle curve
231 (Figure S6). Moreover, the monthly distributions of detrended $r(\text{NDVI}, \text{NBR})$ values closely
232 follow variations in greenness in the double-crop cycle, with greater correlation during seasons
233 of crop growth. This pattern of correlation suggests that the performance of NDVI depends on
234 the level of greenness in-field and that NDVI values at or near-minimum greenness should be
235 interpreted with caution.

236 3.3 Trends in post-monsoon regional aerosol optical depth

237 To quantify the consequences of the delays in post-monsoon agricultural fire activity for
238 regional air quality, we assess AOD exceedances during the main burning period bounded by
239 $x(\text{FRP})_{\text{start}}$ and $x(\text{FRP})_{\text{end}}$. Within this window, post-monsoon AOD exceedances have
240 increased by 50% from 2003-2016, likely associated with the reported upward trend in fire
241 intensity (Figure 4). Similar to the magnitude of the delay in $x(\text{FRP})_{\text{peak}}$, the timing of the peak
242 in AOD, $x(\text{AOD})_{\text{peak}}$, has shifted by $0.82 \text{ days yr}^{-1}$ (95% CI: [0.46, 1.16]), or ~ 12 days during
243 the 14-year period. The delay and increase in post-monsoon agricultural fire activity appear to
244 drive the coherent shifting pattern in heavy aerosol loading episodes (higher AOD exceedances),

245 despite the variability in AOD impacted by meteorology and other pollution sources, such as
246 fireworks during the Diwali festival.

247 **4. Discussion**

248 *4.1 Implications of delays in post-monsoon fire activity*

249 We find that the peak fire intensity of the post-monsoon burning season in Punjab has
250 shifted later in time by over two weeks from 2003 to 2016, with a 40% increase in overall fire
251 intensity. This delay is gradual, likely influenced by steady increases in crop production and
252 mechanization, which yield higher amounts of excess crop residue. We hypothesize that a
253 shortened harvest-to-sowing turnaround time after *kharif* rice harvests has amplified this increase
254 by making it difficult for farmers to prepare fields for timely sowing of *rabi* wheat. The optimal
255 time to sow wheat in Punjab is late October to early November (Liu *et al* 2019, Balwinder-Singh
256 *et al* 2016), yet co-occurring post-monsoon fires indicate that fields are often not ready at this
257 time, particularly in recent years. Since fire is a quick and cheap method to remove the leftover
258 residue generated by combine harvesters, farmers may have even greater incentive to burn crop
259 residue, especially if harvests are delayed past the optimal date to sow wheat. Consistent with
260 this hypothesis, we find that high fire intensity days preferentially occur during the latter half of
261 the fire season, when the optimal window for sowing is shrinking.

262 We also hypothesize that as post-monsoon fires increase in response to mechanization
263 and pressures to sow on time, the burning season gradually trends later, further compressing the
264 harvest-to-sowing window and increasing fire intensity rates. As a result, winter wheat sow dates
265 across the region will likely homogenize, collapsing around a small window to mitigate crop
266 losses from increasing temperatures later in the winter growing season (Lobell *et al* 2012).
267 Additionally, we estimate a 50% increase in regional AOD exceedances and ~12-day delay in the
268 timing peak AOD within the post-monsoon burning period from 2003-2016. Delays in the post-
269 monsoon burning season also suggest that high fire days may increasingly coincide with late-
270 autumn/winter meteorological conditions that favor severe fog/smog and haze events across the
271 IGP (Dey 2018). Dense fog formation peaks in winter (December to January) over the IGP (Dey
272 2018, Gautam and Singh 2018, Ghude *et al* 2017), but in recent years there appears to be an
273 increasing tendency in dense fog episodes observed earlier in November, coinciding with the
274 buildup of intense smoke associated with crop residue burning activity (Figure S7). Aside from
275 increasing exposure to high regional PM both locally and in urban centers downwind, crop
276 residue burning depletes soil moisture and decreases roadside visibility (Kumar *et al* 2015,
277 Badarinath *et al* 2006, Sidhu *et al* 2015, Sinha *et al* 2015). In spite of bans, such burning
278 continues to persist and gain traction (Tallis *et al* 2017). New technology that simultaneously
279 reuses crop residue as mulch cover and incorporates seeds into the bare soil has been tested as an
280 alternative to slash-and-burn methods of managing crop residue (Sidhu *et al* 2015, Tallis *et al*
281 2017).

282 *4.2 Potential drivers of delays in the rice-wheat rotation*

283 Delays in the post-monsoon burning season are consistent with such shifts in the timing
284 of monsoon peak greenness (11-15 days) and post-monsoon trough greenness (4-6 days), though
285 of lesser magnitude. Unlike the steady shifts seen in post-monsoon burning, an abrupt delay of
286 roughly one week occurring around 2008-09 dominates the overall delay in the timing of

287 monsoon peak greenness, with relatively little change thereafter. Abrupt delays of similar
288 magnitude are also apparent in the timing of the start of the post-monsoon burning season. Here
289 we consider whether policy changes implemented around this time may have contributed toward
290 these abrupt shifts. In 2009, in order to counteract severe groundwater depletion driven by low
291 monsoon rainfall and widespread agricultural intensification, the Government of Punjab enacted
292 the "Preservation of Sub-Soil Water Act" (ordinance in 2008), which prohibits sowing rice
293 nurseries before May 10 and transplanting the resulting rice seedlings to flooded paddies before
294 June 10 (Ramanathan *et al* 2005, Asoka *et al* 2017, Singh 2009, Tripathi *et al* 2016). The Act
295 delays the onset of water-intensive agricultural practices that would otherwise coincide with
296 warm temperatures and high pre-monsoon evapotranspiration rates, which lead to excessive
297 usage of the groundwater supply from tube wells and other reservoirs (Humphreys *et al* 2010).

298 Another policy that could be related to the shift is the all-India implementation of the
299 Mahatma Gandhi National Rural Employment Guarantee Act (MGNREGA), a measure that
300 provides a social security net to rural workers (Reddy *et al* 2014) and may have decreased the
301 seasonal migration of workers to Punjab and led to labor shortages there (Singh 2009). Such
302 shortages may have delayed the sowing of rice and incentivized use of combine harvesters,
303 which may in turn explain the increase in crop residue burning. However, the already widespread
304 transition to mechanized harvesting in Punjab, with diminishing dependence on manual labor,
305 suggests that MGNREGA may have had a smaller impact on the timing of harvest and burning.
306 Finally, variations in the timing of monsoon onset may also be partly responsible for the
307 interannual variability in these observed shifts. **Figure S8** summarizes the potential drivers and
308 implications of the delay in and amplification of post-monsoon fire activity associated with
309 double-crop cycle.

310 **5. Conclusion**

311 In summary, we show robust, statistically significant temporal shifts of over two weeks in
312 the timing of peak fire activity during the post-monsoon burning period in Punjab over a 14-year
313 period from 2003-2016, and smaller delays of 9-11 days in monsoon peak greenness and 3-6
314 days in post-monsoon trough greenness. We estimate the start, midpoint, and end of the burning
315 season using FRP as weights and the timing of peak FRP and regional AOD exceedances by
316 optimizing the Gaussian mean. We further demonstrate the viability and applicability of using
317 daily MODIS surface reflectance to characterize crop cycles and the utility of NBR as a useful
318 complement to NDVI. We hypothesize that while the gradual delays in the post-monsoon
319 burning season are likely linked to agricultural intensification and increasing mechanization, the
320 abrupt delay of one week around 2008-09 seen in the monsoon crop growing season appears to
321 coincide with groundwater and labor policy changes. The unintended consequences of these
322 temporal shifts in the double-crop cycle may be severe. First, a shortened harvest-to-sowing
323 period may further encourage farmers to burn crop residues in order to sow winter wheat on
324 time. Second, the timing of peak crop residue burning may increasingly coincide with winter
325 meteorology that favors severe smog events downwind across the IGP, where we diagnose a
326 50% increase in AOD exceedances, defined as the increment of AOD above the mean + 1σ , over
327 2003-2016. Alternative technology that combines the co-benefits of incorporating wheat seeds
328 with rice residue and eliminating the need to burn residue, as well as switching to less water-
329 intensive and stubble-producing crops, may alleviate the double bind of having to conserve
330 groundwater while reducing public health exposure to smoke from post-monsoon fires.

331 **Data Availability**

332 All satellite-derived data used in this study are publicly available. MODIS-derived datasets can
333 be accessed through NASA Earthdata (<https://search.earthdata.nasa.gov/>) and Google Earth
334 Engine (Gorelick *et al* 2017) (<https://earthengine.google.com/>). The Global Fire Emissions
335 Dataset, version 4s, (GFEDv4s) and MODIS and VIIRS active fire geolocations are available
336 from GFED (<http://www.globalfiredata.org/>), University of Maryland
337 (<http://fuoco.geog.umd.edu/>), and NASA Fire Information for Resource Management System
338 (FIRMS) (<https://firms.modaps.eosdis.nasa.gov/>).

339 **Acknowledgements**

340 We thank Marena Lin and Peter Huybers for key contributions to early versions of this work (Liu
341 *et al* 2018a) and Meghna Agarwala for helpful discussions regarding this manuscript. This work
342 was supported by a National Science Foundation Graduate Research Fellowship awarded to T.L.
343 (DGE1745303).

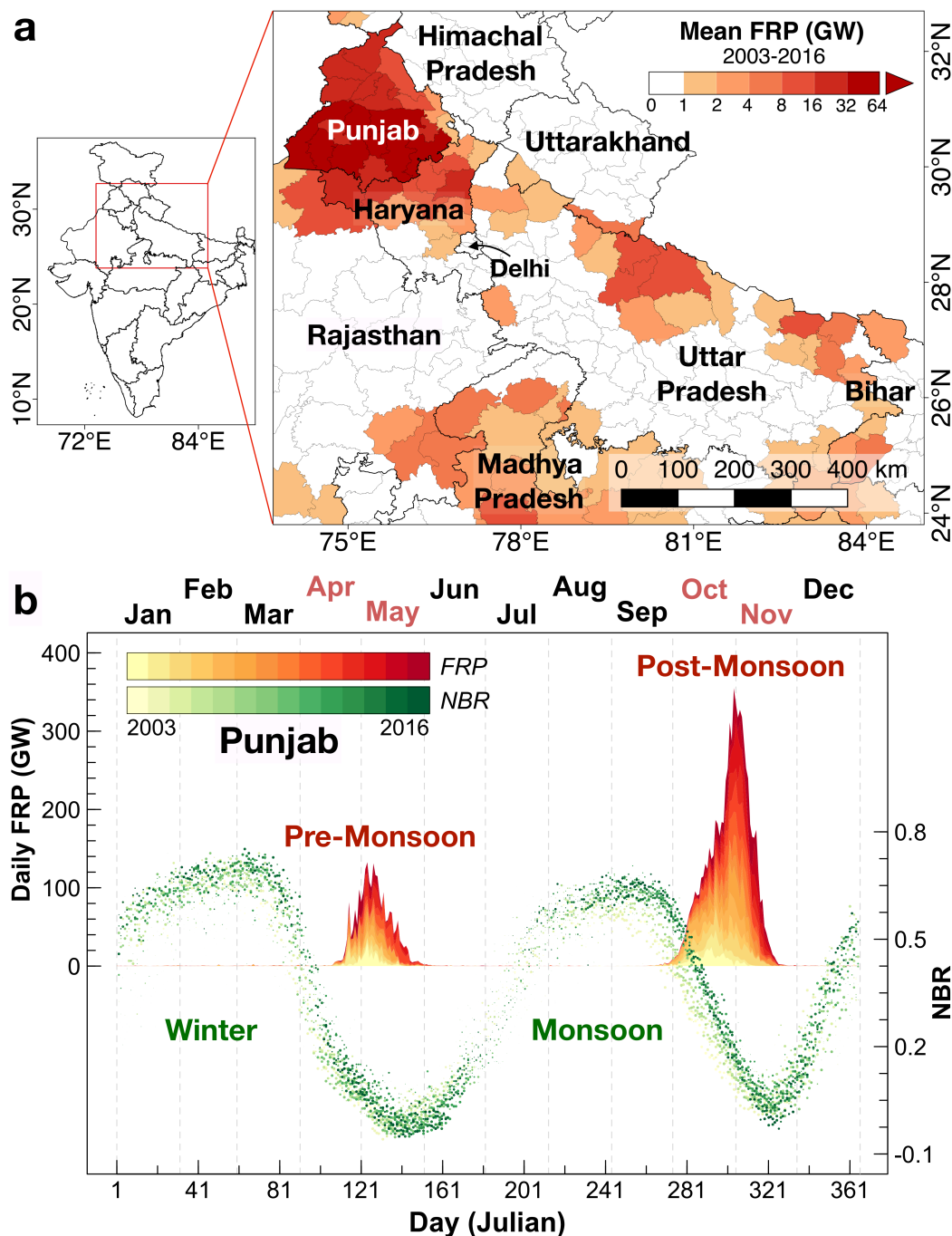
344 **References**

- 345 Amann M, Purohit P, Bhanarkar A D, Bertok I, Borken-Kleefeld J, Cofala J, Heyes C,
346 Kieseewetter G, Klimont Z, Liu J, Majumdar D, Nguyen B, Rafaj P, Rao P S, Sander R,
347 Schöpp W, Srivastava A and Vardhan B H 2017 Managing future air quality in megacities:
348 A case study for Delhi *Atmos. Environ.* **161** 99–111 Online:
349 <https://doi.org/10.1016/j.atmosenv.2017.04.041>
- 350 Asner G P and Lobell D B 2000 A Biogeophysical Approach for Automated SWIR Unmixing of
351 Soils and Vegetation *Remote Sens. Environ.* **74** 99–112 Online:
352 [https://doi.org/10.1016/S0034-4257\(00\)00126-7](https://doi.org/10.1016/S0034-4257(00)00126-7)
- 353 Asoka A, Gleeson T, Wada Y and Mishra V 2017 Relative contribution of monsoon precipitation
354 and pumping to changes in groundwater storage in India *Nat. Geosci.* **10** 109–17 Online:
355 <https://doi.org/10.1038/ngeo2869>
- 356 Avery T E and Berlin G L 1992 *Fundamentals of remote sensing and airphoto interpretation*
357 (New York, NY: Macmillan Publishing Company)
- 358 Azzari G, Jain M and Lobell D B 2017 Towards fine resolution global maps of crop yields:
359 Testing multiple methods and satellites in three countries *Remote Sens. Environ.* **202** 129–
360 41 Online: <http://dx.doi.org/10.1016/j.rse.2017.04.014>
- 361 Badarinath K V S, Kiran Chand T R and Krishna Prasad V 2006 Agriculture crop residue
362 burning in the Indo-Gangetic Plains - A study using IRS-P6 AWiFS satellite data *Curr. Sci.*
363 **91** 1085–9
- 364 Balwinder-Singh, Humphreys E, Gaydon D S and Eberbach P L 2016 Evaluation of the effects
365 of mulch on optimum sowing date and irrigation management of zero till wheat in central
366 Punjab, India using APSIM *F. Crop. Res.* **197** 83–96 Online:
367 <http://dx.doi.org/10.1016/j.fcr.2016.08.016>
- 368 Chen D, Huang J and Jackson T J 2005 Vegetation water content estimation for corn and
369 soybeans using spectral indices derived from MODIS near- and short-wave infrared bands
370 *Remote Sens. Environ.* **98** 225–36 Online: <https://doi.org/10.1016/j.rse.2005.07.008>

- 371 Choudhury S, Rajpal H, Saraf A K and Panda S 2007 Mapping and forecasting of North Indian
372 winter fog: an application of spatial technologies *Int. J. Remote Sens.* **28** 3649–63 Online:
373 <https://doi.org/10.1080/01431160600993470>
- 374 Cusworth D H, Mickley L J, Sulprizio M P, Liu T, Marlier M E, DeFries R S, Guttikunda S K
375 and Gupta P 2018 Quantifying the influence of agricultural fires in northwest India on urban
376 air pollution in Delhi, India *Environ. Res. Lett.* **13** 044018 Online:
377 <https://doi.org/10.1088/1748-9326/aab303>
- 378 Dey S 2018 On the theoretical aspects of improved fog detection and prediction in India *Atmos.*
379 *Res.* **202** 77–80 Online: <https://doi.org/10.1016/j.atmosres.2017.11.018>
- 380 Eva H and Lambin E F 1998 Burnt area mapping in Central Africa using ATSR data *Int. J.*
381 *Remote Sens.* **18** 3473–97 Online: <https://doi.org/10.1080/014311698213768>
- 382 Gautam R and Singh M K 2018 Urban Heat Island Over Delhi Punches Holes in Widespread
383 Fog in the Indo-Gangetic Plains *Geophys. Res. Lett.* **45** Online:
384 <https://doi.org/10.1002/2017GL076794>
- 385 Ghude S D, Bhat G S, Prabhakaran T, Jenamani R K, Chate D M, Safai P D, Karipot A K,
386 Konwar M, Pithani P, Sinha V, Rao P S P, Dixit S A, Tiwari S, Todekar K, Varpe S,
387 Srivastava A K, Bisht D S, Murugavel P, Ali K, Mina U, Dharua M, Jaya Rao Y,
388 Padmakumari B, Hazra A, Nigam N, Shende U, Lal D M, Chandra B P, Mishra A K,
389 Kumar A, Hakkim H, Pawar H, Acharja P, Kulkarni R, Subharthi C, Balaji B, Varghese M,
390 Bera S and Rajeevan M 2017 Winter fog experiment over the Indo-Gangetic plains of India
391 *Curr. Sci.* **112** 767–84 Online: <https://doi.org/10.18520/cs/v112/i04/767-784>
- 392 Gorelick N, Hancher M, Dixon M, Ilyushchenko S, Thau D and Moore R 2017 Google Earth
393 Engine: Planetary-scale geospatial analysis for everyone *Remote Sens. Environ.* **202** 18–27
394 Online: <https://doi.org/10.1016/j.rse.2017.06.031>
- 395 Humphreys E, Kukal S S, Christen E W, Hira G S, Balwinder-Singh, Sudhir-Yadav and Sharma
396 R K 2010 Halting the groundwater decline in north-west india-which crop technologies will
397 be winners? *Adv. Agron.* **109** 155–217
- 398 Jain M, Mondal P, DeFries R S, Small C and Galford G L 2013 Mapping cropping intensity of
399 smallholder farms: A comparison of methods using multiple sensors *Remote Sens. Environ.*
400 **134** 210–23 Online: <http://dx.doi.org/10.1016/j.rse.2013.02.029>
- 401 Jain M, Mondal P, Galford G, Fiske G and DeFries R 2017 An Automated Approach to Map
402 Winter Cropped Area of Smallholder Farms across Large Scales Using MODIS Imagery
403 *Remote Sens.* **9** 566 Online: <http://www.mdpi.com/2072-4292/9/6/566>
- 404 Jethva H, Chand D, Torres O, Gupta P, Lyapustin A and Patadia F 2018 Agricultural Burning
405 and Air Quality over Northern India: A Synergistic Analysis using NASA's A-train Satellite
406 Data and Ground Measurements *Aerosol Air Qual. Res.* **18** 1756–73 Online:
407 <http://doi.org/10.4209/aaqr.2017.12.0583>
- 408 Justice C O, Townshend J R G, Holben B N and Tucker C J 1985 Analysis of the phenology of
409 global vegetation using meteorological satellite data *Int. J. Remote Sens.* **6** 1271–318
410 Online: <https://doi.org/10.1080/01431168508948281>
- 411 Kaskaoutis D G, Kumar S, Sharma D, Singh R P, Kharol S K, Sharma M, Singh A K, Singh S,
412 Singh A and Singh D 2014 Effects of crop residue burning on aerosol properties, plume
413 characteristics, and long-range transport over northern India *J. Geophys. Res. Atmos.* **119**

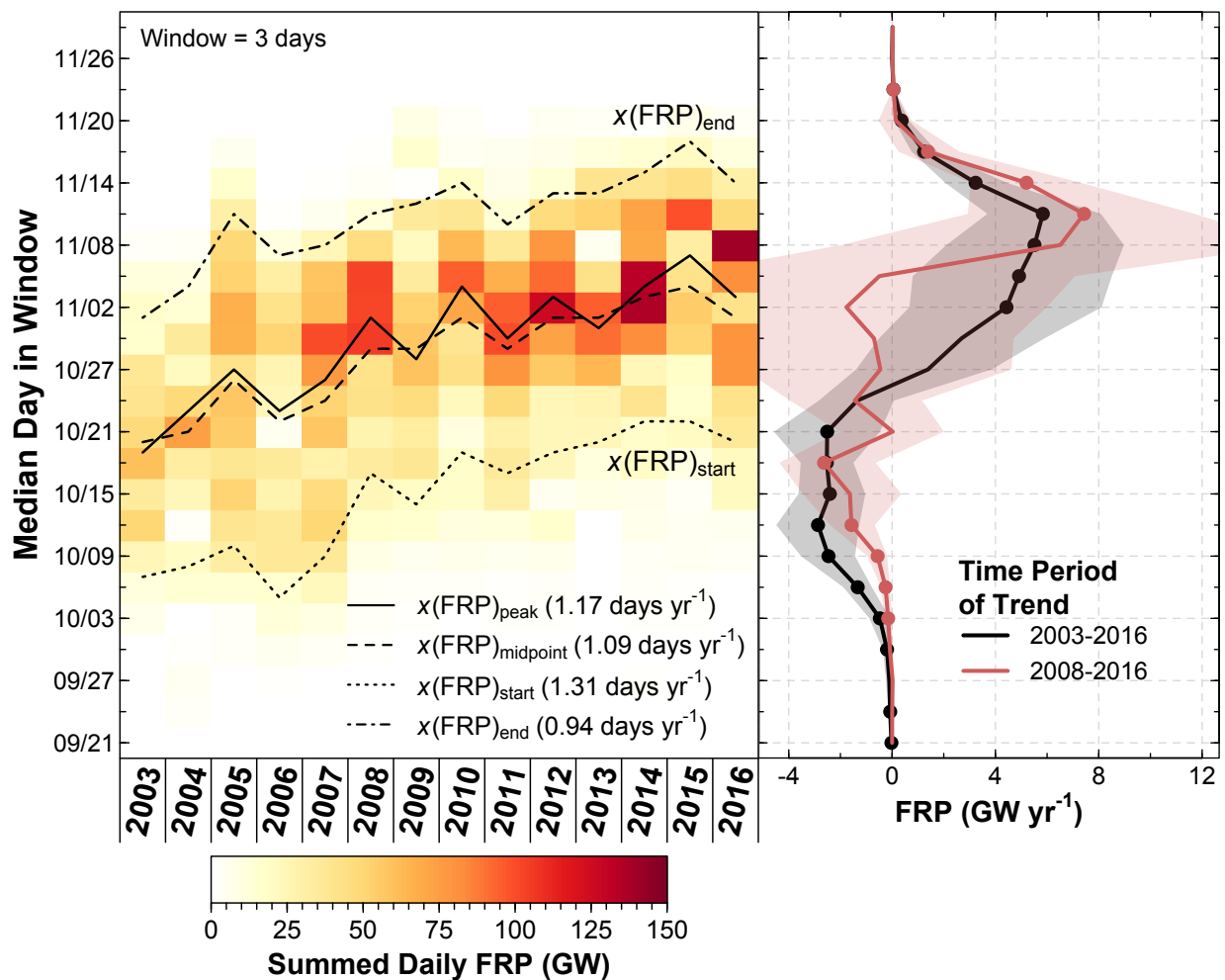
- 414 5424–44 Online: <https://doi.org/10.1002/2013JD021357>
- 415 Key C H and Benson N C 2006 *Landscape Assessment (LA)*. In: Lutes, Duncan C.; Keane,
416 Robert E.; Caratti, John F.; Key, Carl H.; Benson, Nathan C.; Sutherland, Steve; Gangi,
417 Larry J. 2006. *FIREMON: Fire effects monitoring and inventory system* Online:
418 https://www.fs.fed.us/rm/pubs/rmrs_gtr164/rmrs_gtr164_13_land_assess.pdf
- 419 Kumar P, Kumar S and Joshi L 2015 *Socioeconomic and Environmental Implications of*
420 *Agricultural Residue Burning: A Case Study of Punjab, India* Online:
421 <https://doi.org/10.1007/978-81-322-2014-5>
- 422 Liu T, Lin M, Mickley L J, Huybers P, Gautam R, Singh M K, DeFries R S and Marlier M E
423 2018a Consequences for regional air quality from temporal shifts in post-monsoon
424 agricultural burning associated with the double-crop cycle of Punjab, India *American*
425 *Geophysical Union Fall Meeting* Online:
426 <https://agu.confex.com/agu/fm18/meetingapp.cgi/Paper/431161>
- 427 Liu T, Marlier M E, DeFries R S, Westervelt D M, Xia K R, Fiore A M, Mickley L J, Cusworth
428 D H and Milly G 2018b Seasonal impact of regional outdoor biomass burning on air
429 pollution in three Indian cities: Delhi, Bengaluru, and Pune *Atmos. Environ.* **172** 83–92
430 Online: <https://doi.org/10.1016/j.atmosenv.2017.10.024>
- 431 Liu T, Marlier M E, Karambelas A, Jain M, Singh S, Singh M K, Gautam R and DeFries R S
432 2019 Missing emissions from post-monsoon agricultural fires in northwestern India:
433 regional limitations of MODIS burned area and active fire products *Environ. Res. Commun.*
434 **1** 011007 Online: <https://doi.org/10.1088/2515-7620/ab056c>
- 435 Lobell D B, Ortiz-Monasterio J I, Sibley A M and Sohu V S 2013 Satellite detection of earlier
436 wheat sowing in India and implications for yield trends *Agric. Syst.* **115** 137–43 Online:
437 <http://dx.doi.org/10.1016/j.agry.2012.09.003>
- 438 Lobell D B, Sibley A and Ivan Ortiz-Monasterio J 2012 Extreme heat effects on wheat
439 senescence in India *Nat. Clim. Chang.* **2** 186–9 Online:
440 <http://dx.doi.org/10.1038/nclimate1356>
- 441 Mondal P, Jain M, DeFries R S, Galford G L and Small C 2015 Sensitivity of crop cover to
442 climate variability: Insights from two Indian agro-ecoregions *J. Environ. Manage.* **148** 21–
443 30 Online: <http://dx.doi.org/10.1016/j.jenvman.2014.02.026>
- 444 Mondal P, Jain M, Robertson A W, Galford G L, Small C and DeFries R S 2014 Winter crop
445 sensitivity to inter-annual climate variability in central India *Clim. Change* **126** 61–76
- 446 Ramanathan V, Chung C, Kim D, Bettge T, Buja L, Kiehl J T, Washington W M, Fu Q, Sikka D
447 R and Wild M 2005 Atmospheric brown clouds: Impacts on South Asian climate and
448 hydrological cycle *Proc. Natl. Acad. Sci.* **102** 5326–33 Online:
449 <https://doi.org/10.1073/pnas.0500656102>
- 450 Reddy D N, Reddy A A and Bantilan M C S 2014 The impact of Mahatma Gandhi National
451 Rural Employment Guarantee Act (MGNREGA) on rural labor markets and agriculture
452 *India Rev.* **13** 251–73
- 453 Roy D P, Giglio L, Kendall J D and Justice C O 1999 Multi-temporal active-fire based burn scar
454 detection algorithm *Int. J. Remote Sens.* **20** 1031–8 Online:
455 <https://doi.org/10.1080/014311699213073>

- 456 Saraf A, Bora A, Das J, Rawat V, Sharma K and Jain S K 2010 Winter fog over the Indo-
457 Gangetic Plains: Mapping and modelling using remote sensing and GIS *Nat. Hazards* **52**
458 199–220 Online: <https://doi.org/10.1007/s11069-010-9660-0>
- 459 Sidhu H S, Singh M, Yadvinder S, Blackwell J, Lohan S K, Humphreys E, Jat M L, Singh V and
460 Singh S 2015 Development and evaluation of the Turbo Happy Seeder for sowing wheat
461 into heavy rice residues in NW India *F. Crop. Res.* **184** 201–12 Online:
462 <https://doi.org/10.1016/j.fcr.2015.07.025>
- 463 Singh K 2009 Act to Save Groundwater in Punjab: Its Impact on Water Table, Electricity
464 Subsidy and Environment *Agric. Econ. Res. Rev.* **22** 365–386
- 465 Sinha B, Singh Sangwan K, Maurya Y, Kumar V, Sarkar C, Chandra B P and Sinha V 2015
466 Assessment of crop yield losses in Punjab and Haryana using 2 years of continuous in situ
467 ozone measurements *Atmos. Chem. Phys.* **15** 9555–76
- 468 Tallis H, Polasky S, Shyamsundar P, Springer N, Ahuja V, Cummins J, Datta I, Dixon J, Gerard
469 B, Ginn W, Gupta R, Jadhav A, Jat M, Keil A, Krishnapriya P, Ladha J, Nandrajog S, Paul
470 S, Lopez Ridaura S, Ritter A, Sidhu H, Skiba N and Somanathan R 2017 *The Evergreen*
471 *Revolution: Six Ways to empower India's no-burn agricultural future* Online:
472 <https://www.nature.org/science-in-action/the-evergreen-revolution.pdf>
- 473 Thumaty K C, Rodda S R, Singhal J, Gopalakrishnan R, Jha C S, Parsi G D and Dadhwal V K
474 2015 Spatio-temporal characterization of agriculture residue burning in Punjab and
475 Haryana, India, using MODIS and Suomi NPP VIIRS data *Curr. Sci.* **109** 1850–5 Online:
476 <https://doi.org/10.18520/v109/i10/1850-1855>
- 477 Tripathi A, Mishra A K and Verma G 2016 Impact of Preservation of Subsoil Water Act on
478 Groundwater Depletion: The Case of Punjab, India *Environ. Manage.* **58** 48–59
- 479 Yengoh G T, Dent D, Olsson L, Tengberg A E and Tucker C J 2015 *Use of the Normalized*
480 *Difference Vegetation Index (NDVI) to Assess Land Degradation at Multiple Scales:*
481 *Current Status, Future Trends, and Practical Considerations* (Springer International
482 Publishing)
- 483 Zhao H, Yang Z, Di L, Li L and Zhu H 2009 Crop phenology date estimation based on NDVI
484 derived from the reconstructed MODIS daily surface reflectance data 2009 *17th Int. Conf.*
485 *Geoinformatics* 3–8

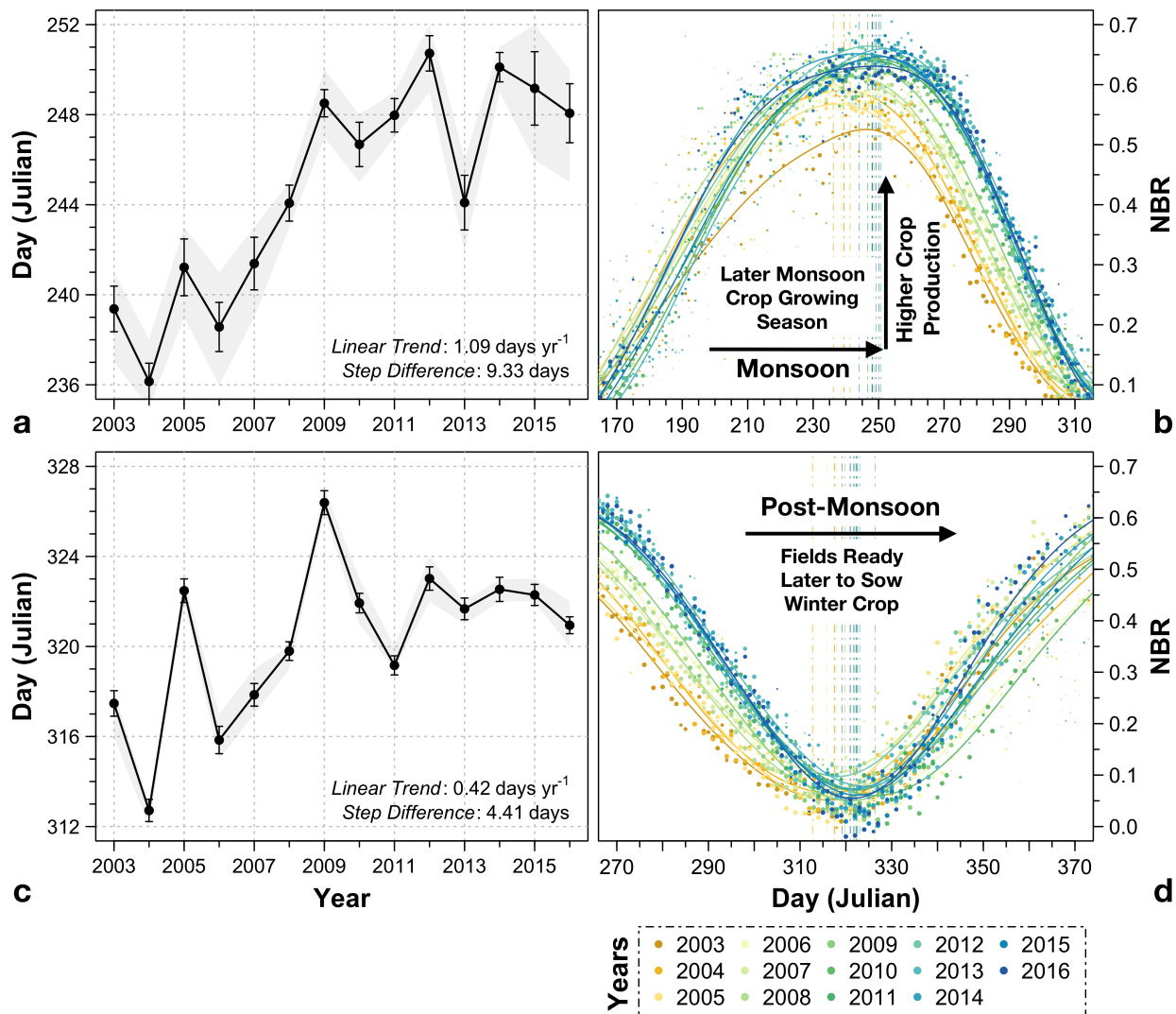


486

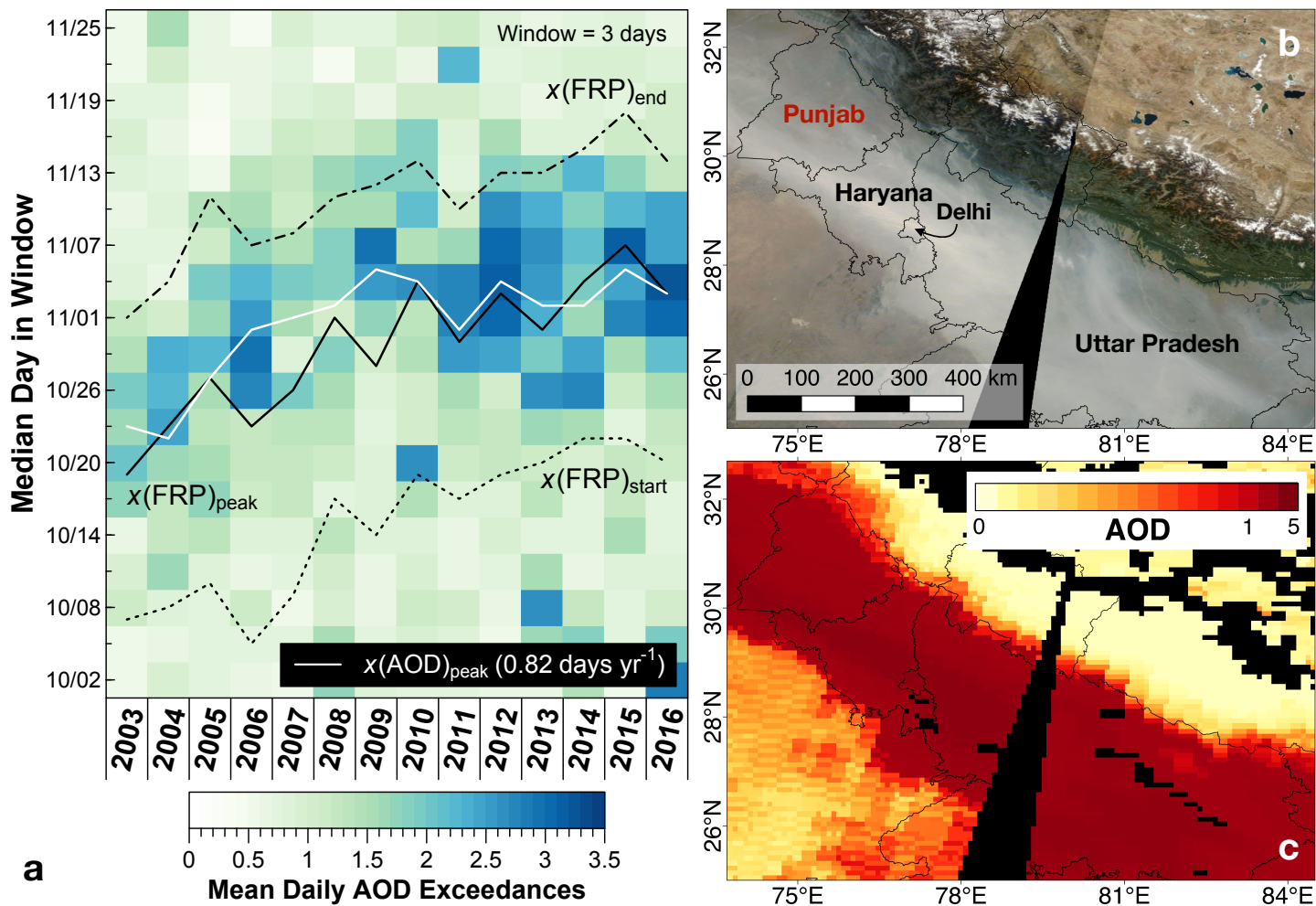
487 **Figure 1. Cycles of fire activity and vegetation greenness in Punjab, India.** District-level
 488 maps of (a) the Indo-Gangetic Plain (IGP) overlaid with annual agricultural MODIS Aqua +
 489 Terra Fire Radiative Power (GW), averaged over 2003-2016. (b) Daily FRP (left axis) and
 490 median Normalized Burn Ratio (NBR; right axis) in Punjab. FRP values are stacked with earlier
 491 years on the bottom. The double-crop cycle indicated by NBR, a proxy for greenness, is
 492 predominantly a rice-wheat rotation. Pre-monsoon fires occur from April to May after the winter
 493 wheat growing season, and post-monsoon fires occur from October to November after the
 494 monsoon rice growing season.



495
 496 **Figure 2. Temporal shifts in post-monsoon fires in Punjab from 2003-2016.** (left) Each block
 497 represents the 3-day summed Fire Radiative Power (FRP). Dashed and solid lines represent the
 498 timing of the start, peak, midpoint, and end of the post-monsoon burning season, based on daily
 499 observations of FRP. Text inset in the left panel shows the linear trends in the $x(FRP)_{start}$,
 500 $x(FRP)_{peak}$, $x(FRP)_{midpoint}$, and $x(FRP)_{end}$; all trends shown are statistically significant at
 501 the 95% confidence level. (right) Trends in summed FRP (GW yr^{-1}) for each 3-day block
 502 window from September 20 to November 30 for the 2003-2016 (black line) and 2008-2016 time
 503 periods (red line). The shaded envelopes denote the 95% confidence interval, and dots represent
 504 statistically significant increases or decreases in 3-day block FRP.



505
 506 **Figure 3. Trends in monsoon peak greenness and post-monsoon trough greenness in**
 507 **Punjab from 2003-2016.** Bootstrapped mean maximum NBR during the (a) monsoon crop
 508 growing season and (c) post-monsoon harvest season, from 2003-2016. Error bars show one σ
 509 uncertainty, and shaded gray envelopes denote the 95% confidence interval. Text inset shows the
 510 bootstrapped linear trend in the timing of (a) maximum monsoon greenness and (c) minimum
 511 post-monsoon greenness from 2003-2016 and mean step difference between the 2003-2007 and
 512 2008-2016 time periods. Daily median NBR during the (b) monsoon crop growing season and
 513 (d) post-monsoon harvest season, with lines showing the weighted parabola smoothing. Different
 514 colors denote different years. The bootstrapped mean day of (b) maximum monsoon greenness
 515 and (d) minimum post-monsoon greenness of each year is shown by vertical dashed-dot lines.



517 **Figure 4. Trend in the timing of peak post-monsoon AOD over the western Indo-Gangetic**
 518 **Plain from 2003-2016.** (a) Each block represents the 3-day average of regional aerosol optical
 519 depth (AOD) exceedances from the MODIS/Terra Deep Blue retrieval algorithm over Punjab,
 520 Haryana, Delhi, and western Uttar Pradesh. Here exceedances are defined as the spatially
 521 averaged AOD increments above the mean AOD + 1σ for each season and pixel. Dashed lines
 522 represent the timing of the start, peak, and end of the post-monsoon burning season, based on
 523 daily FRP (same as in Figure 2). Text shows the linear trend in the $x(\text{AOD})_{\text{peak}}$, statistically
 524 significant at the 95% confidence level. Example of thick haze over the western IGP on
 525 November 6, 2016, as observed by MODIS/Terra, shown as (b) true color and (c) Deep Blue
 526 AOD (NASA/Worldview; <https://worldview.earthdata.nasa.gov/>). The colorbar in (c) is
 527 logarithmic.